remote sensing

MDPI

Article

5-Minute Water Level Retrieval and Dynamic Responses to Water-Sediment Regulation from GNSS-IR in the Yellow River

Yuanmao Fan [1], Shuanggen Jin [1,2,*] and Lei Hong [1,3]

[1] School of Surveying and Land Information Engineering, Henan Polytechnic University, Jiaozuo 454003, China; 212304010023@home.hpu.edu.cn (Y.F.); lei.hong@edu.uah.es (L.H.)
[2] School of Artificial Intelligence, Anhui University, Hefei 230601, China
[3] Department of Physics and Mathematics, University of Alcala, 28801 Alcala de Henares, Spain
* Correspondence: sgjin@hpu.edu.cn or sg.jin@yahoo.com

Highlights

What are the main findings?

- A high temporal resolution water level estimation framework with a 5-minute interval was developed by integrating 40-minute sliding-window processing, variational mode decomposition (VMD), and multi-GNSS-IR in Yellow River.
- The method performed well at both Huayuankou and Xiaolangdi, and the two stations' records revealed an about 21-h downstream lag and clear flood-wave attenuation during the 2025 water-sediment regulation event.

What are the implications of the main findings?

- The study develops a high-frequency GNSS-IR water level retrieval from traditional low-frequency arc-based estimation to continuous and high temporal resolution estimation in both wandering and canyon-controlled river reaches.
- The GNSS-IR estimated water level time series with a 5-minute interval can support dynamic response analysis, flood-wave tracking, and water regulation management in complex inland rivers.

Abstract

Accurate and continuous high-frequency water level monitoring is essential for flood control, water resource regulation, and hydrological studies in the Yellow River. However, traditional methods are often limited in complex inland river environments with insufficient temporal resolution, poor continuity, and weak robustness. In this study, high-frequency water level changes and their dynamic responses to water-sediment regulation were estimated at Huayuankou and Xiaolangdi stations based on a sliding window, variational mode decomposition (VMD), and multi-GNSS interferometric reflectometry (GNSS-IR). The results show that high-temporal-resolution water level series with a 5-minute interval were achieved at Huayuankou and Xiaolangdi. When compared with in situ gauge measurements, the GNSS-IR estimated water level has a root mean square error (RMSE) of 0.09 and 0.14 m, and coefficient of determination (R^2) values with 0.92 and 0.96, respectively. These results demonstrated strong effects by reservoir regulation in both wide-and-shallow wandering reaches and canyon-controlled reaches. Water level responses to the 2025 water-sediment regulation operation showed that Xiaolangdi responded rapidly to upstream reservoir releases, whereas Huayuankou exhibited a delayed response, with the flood peak arriving about 21 h later and attenuating during downstream propagation. The proposed method shows strong potential for high-frequency water level monitoring and dynamic response analysis from GNSS-IR in complex inland rivers.

Check for updates

Academic Editor: Chung-yen Kuo

Received: 14 April 2026
Revised: 20 May 2026
Accepted: 22 May 2026
Published: 2 June 2026

Copyright: © 2026 by the authors. Licensee MDPI, Basel, Switzerland. This article is an open access article distributed under the terms and conditions of the Creative Commons Attribution (CC BY) license.

Keywords: GNSS-IR; Yellow River; water level; sliding window; dynamic response

1. Introduction

The Yellow River, the second longest river in China, exhibits water level variations that serve not only as a crucial scientific basis for basin-scale flood control, disaster mitigation, water resource regulation, and ecological protection, but also as a key hydrological indicator for understanding complex channel evolution and the impacts of human intervention [1]. However, the water-sediment dynamics in the middle and lower reaches of the river are highly complex, characterized by intense local scour and deposition, as well as pronounced temporal variability and abruptness in water level processes. Although traditional in situ monitoring methods—such as manual staff gauges, buoys, and pressure-based electronic water gauges—have long supported hydrological operations, they suffer from high construction and maintenance costs, limited spatial coverage, and significant sensitivity to high flow velocities and floating debris [2]. On the other hand, rapidly advancing satellite radar altimetry enables large-scale water level observation [3], but its long revisit cycle, insufficient temporal resolution, and vulnerability to land-contaminated echoes over small- to medium-sized wide-and-shallow inland rivers [4] hinder its ability to achieve high-frequency, continuous dynamic monitoring under complex hydrological conditions.

Nowadays, Global Navigation Satellite System (GNSS) has been widely used in positioning, navigation and timing as well as space weather [5,6], while GNSS interferometric reflectometry (GNSS-IR) has emerged as a promising microwave remote-sensing technique for hydrological monitoring because of its all-weather capability and non-contact operation. By analyzing the interference oscillations formed by the superposition of direct and surface-reflected signals in receiver signal-to-noise ratio (SNR) observations, GNSS-IR can retrieve reflector height with high precision. Since Martin-Neira et al. first proposed the use of GNSS reflected signals for water-surface altimetry [7], Larson and other scientists further established an SNR-based multipath interference framework for water level retrieval, thereby promoting the continued development of GNSS-IR applications such as tide level monitoring, soil moisture sensing, snow depth estimation, and inland water level retrieval [8–14]. In particular, Larson et al. successfully retrieved coastal sea surface height using a single geodetic GPS receiver, with results highly consistent with tide gauge observations [15]. With the full deployment of GPS, BDS, GLONASS, and Galileo, multi-constellation and multi-frequency GNSS observations now provide more favorable conditions for improving the spatial and temporal coverage of hydrological retrievals. Chen et al. recently demonstrated at the Datong station of the Yangtze River the centimeter-level potential of multi-GNSS GNSS-IR for the high-frequency monitoring of water levels in large inland rivers [16].

Nevertheless, for complex inland hydrological settings such as the wide-and-shallow wandering reaches of the Yellow River under strong anthropogenic regulation, existing GNSS-IR applications still face two major challenges. First, temporal resolution remains insufficient. Conventional GNSS-IR methods typically use complete satellite arcs lasting several hours as a single processing unit, so the retrieved results represent average conditions over relatively long time windows and are therefore unable to capture transient water level fluctuations at hourly or even minute scales during flood seasons or reservoir regulation events. Second, nonstationary multipath noise and gross-error contamination remain pronounced in complex environments. In wide-and-shallow wandering channels, exposed sandbars, riparian vegetation, and irregular banks can introduce substantial non-water diffuse reflections; in canyon-controlled reaches, surrounding mountains, dams, and

local obstructions can further degrade signal quality. Under such conditions, observations from a single constellation or frequency band are easily affected by satellite geometry and local environmental changes, leading to unstable or fluctuating retrieval results. Therefore, achieving high-temporal-resolution and highly robust multi-GNSS water level retrieval in complex riverine environments remains a key challenge.

The transitional reach between the middle and lower Yellow River is not only a critical zone for flood control and water-sediment regulation, but also one of the regions where high-frequency water level monitoring is most urgently needed. In particular, under strong anthropogenic regulation such as water and sediment regulation operations, river-stage processes often exhibit rapid rise and fall, stage-dependent nonstationarity, and downstream propagation simultaneously. If only low-frequency and discrete observations are available, it is difficult to fully characterize the formation, propagation, and attenuation of flood peaks. Therefore, developing high-frequency, continuous, and stable water level monitoring for key control reaches would not only improve the applicability of retrieval methods in complex river environments, but also deepen our understanding of typical Yellow River regulation processes and flood wave propagation mechanisms.

This study jointly investigates two representative control stations in the middle and lower Yellow River: Huayuankou and Xiaolangdi. Huayuankou, located near the starting point of the perched reach in the lower Yellow River, represents a typical wide-and-shallow wandering river environment, where frequent bed scour and deposition, exposed near-bank shoals, and riparian vegetation can easily generate complex non-water diffuse reflections. Xiaolangdi, by contrast, is situated near the outlet of the last canyon reach in the middle Yellow River and serves as a key control station for flood regulation and water-sediment management in the middle and lower basin; its water level variations directly reflect upstream reservoir operation and release processes (Figure 1). The two stations thus form a clear upstream–downstream pair in space, while also representing two contrasting hydrological scenarios: upstream reservoir regulation response and downstream propagation response in a wandering channel. This makes them particularly suitable for simultaneously evaluating the performance of high-frequency GNSS-IR water level retrieval and further analyzing two-station dynamic responses and flood wave propagation during water and sediment regulation.

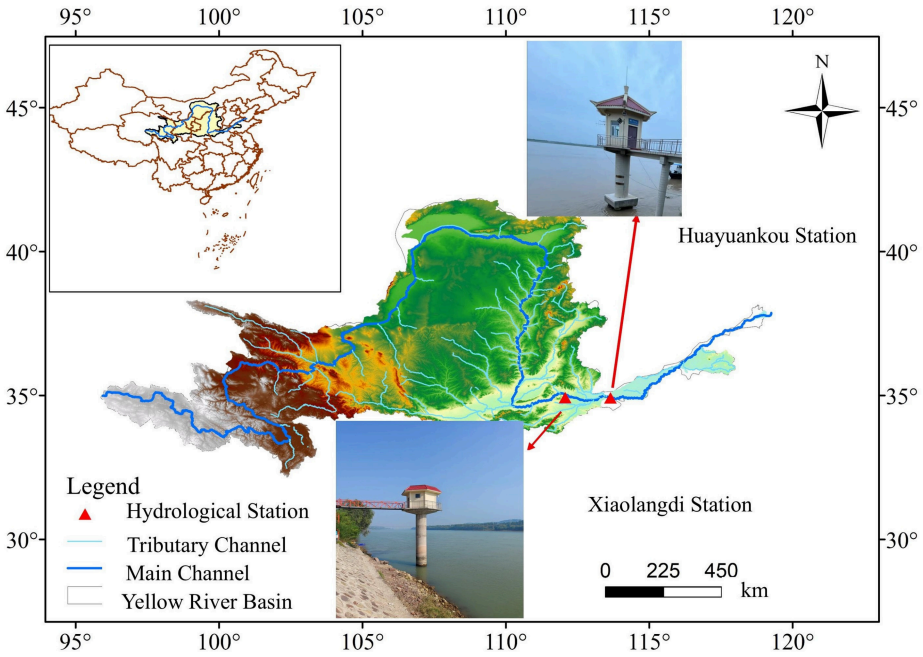


Figure 1. Locations of the Xiaolangdi and Huayuankou stations and their surrounding environments.

Although GNSS-IR has already achieved centimeter-level accuracy in coastal and reservoir water level monitoring [17,18], studies in the wide-and-shallow wandering reaches of the middle and lower Yellow River remain limited because of intense channel scour and deposition and the complexity of bank and shoal environments. From a methodological perspective, variational mode decomposition (VMD) and wavelet decomposition can extract oscillation frequencies from SNR observations. Wang et al. systematically compared three methods under different sampling intervals and found that wavelet decomposition performed best at 1–15-s intervals, whereas the Lomb–Scargle method was least affected at a 30-s interval [19]. Liu et al. further combined wavelet transform with the whale optimization algorithm and improved sea level retrieval performance through the enhanced separation of direct and reflected signals and better parameter estimation [20]. In terms of multi-GNSS integration, Wang et al. showed that combining the four major GNSS constellations significantly improved both the temporal resolution and accuracy of water level series [21], while Chen et al. further verified the feasibility of centimeter-level water level retrieval along the Yangtze main stem using multi-GNSS GNSS-IR [16]. Liu et al. fused GNSS-IR with GNSS positioning to achieve the long-term monitoring of absolute coastal sea level variations and pointed out that retrieval accuracy decreases markedly when reflector height is large [22]. To address the limited number of retrieval points at a single station, Shan et al. proposed a robust multi-station fusion method that suppresses outliers through jointly optimized weighting and improves both model robustness and stability [23]. In addition, Liu et al. successfully retrieved water level variations during flood events using bank-based GNSS equipment and found a 2–5-day lag between rainfall peaks and water level peaks [24]. Preliminary studies in the Yellow River basin include using a low-cost GPS receiver for water level monitoring at Yanguoxia and achieved decimeter-level accuracy [17], and high-precision reservoir water level monitoring using GNSS-IR [18]. However, most existing studies have focused on single-site validation, low-frequency retrievals, or relatively ideal signal environments. Systematic studies on high-frequency dynamic monitoring, two-station response comparison, and flood wave propagation in complex settings, such as the wide-and-shallow wandering reaches and canyon-regulated river sections of the Yellow River, remains lacking. Jin et al. summarized recent advances in GNSS reflectometry and emphasized that multi-constellation integration, high spatiotemporal resolution monitoring, and disaster response applications are major future directions, while refined retrieval over complex inland waters remains a key research frontier [25]. Accordingly, further methodological evaluation and improvement are still needed for high-frequency, high-robustness water level retrieval in strongly regulated Yellow River environments with complex water-sediment conditions.

Recently, sliding-window strategies have been introduced to address the limitations of temporal resolution in conventional GNSS-IR. For instance, Ye et al. successfully achieved 10-minute sea level monitoring using a 40-minute sliding window [26]. More recently, Jin et al. further advanced this framework to a 5- minute temporal resolution in the Yangtze River by integrating a 40-minute sliding window with VMD [8]. Inspired by these proven parameter configurations, this study develops a high-frequency GNSS-IR water level retrieval method based on a sliding window, VMD, and multi-GNSS joint estimation, with aiming to improve the temporal resolution, continuity, and stability of water level retrievals in complex riverine environments. On this basis, high-frequency water level series are further used to analyze stage-dependent dynamic responses and flood wave propagation during water and sediment regulation. Specifically, the objectives of this study are: (1) to develop a high-frequency GNSS-IR water level retrieval framework for the complex inland river environment of the Yellow River and to evaluate its accuracy and stability at the Huayuankou and Xiaolangdi stations; (2) to construct long-term high-frequency water

level series for both stations using a unified methodology, thereby providing a consistent data basis for upstream–downstream process evaluation; and (3) to reveal the dynamic response and flood wave evolution along the Xiaolangdi–Huayuankou reach during water and sediment regulation based on the two-station high-frequency water level records.

2. Materials and Methods

2.1. Datasets and Data Preprocessing

This study focuses on two representative control stations located in the key transitional reach between the middle and lower Yellow River: Huayuankou and Xiaolangdi. Huayuankou is situated near the starting point of the perched reach in the lower Yellow River and represents a typical wide-and-shallow wandering channel, where frequent bed scour and deposition, exposed near-bank shoals, and riparian vegetation can generate strong non-water diffuse reflections and thus pose substantial challenges to GNSS-IR signal extraction and quality control. Xiaolangdi is located near the outlet of the last canyon reach in the middle Yellow River and serves as an important control station for flood control and water-sediment regulation in the middle and lower basin. Its water level variations directly reflect reservoir operation and release processes. The two stations form a clear upstream–downstream pair, with Xiaolangdi located approximately 115 km upstream of Huayuankou, making them well suited for analyzing high-frequency water level variations and the dynamic characteristics of flood wave propagation.

The GNSS observation data used in this study were collected independently at the Xiaolangdi and Huayuankou stations from June 2023 to December 2025. Figure 2a shows the geographical locations of the two sites. Figure 2b,c illustrate the installed antenna and surrounding environment at the Xiaolangdi station, while Figure 2d,e present those at the Huayuankou station. Both stations are equipped with a P5 intelligent GNSS receiver (CHC Navigation, Shanghai, China) connected to an A230GRB geodetic antenna, capable of tracking GPS, GLONASS, Galileo, and BDS signals. Subsequent GNSS-IR data processing and algorithm implementation were performed using MATLAB (v2025b).

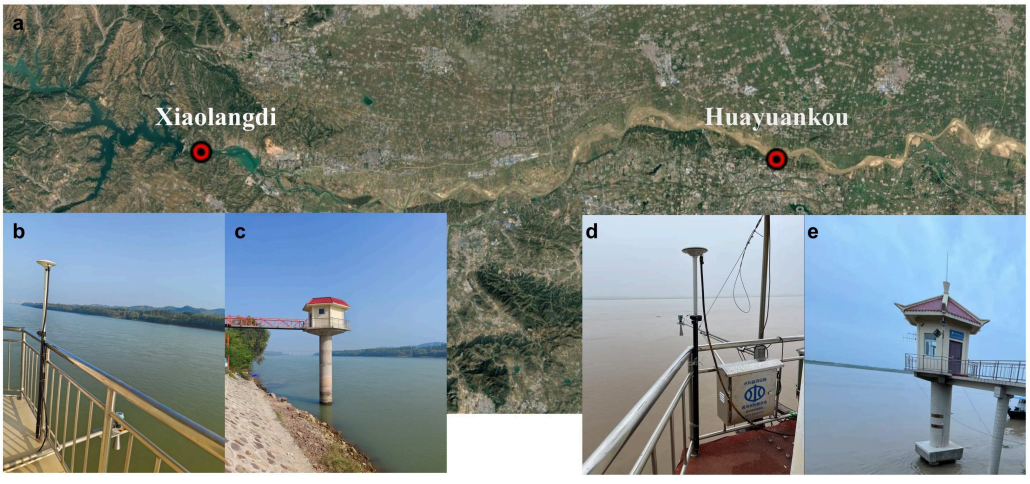


Figure 2. (**a**) Geographic locations of Xiaolangdi and Huayuankou. (**b**,**c**) are antennas and surrounding environments at Xiaolangdi, and (**d**,**e**) are antennas and surrounding environments at Huayuankou stations, respectively.

To support high-frequency water level retrieval and dynamic response analysis at the two stations, multiple datasets were integrated, including GNSS observations, precise orbit products, in situ water level measurements, and ERA5 meteorological reanalysis data. GNSS observations were collected at a sampling rate of 1 Hz and archived in Receiver

Independent Exchange Format (RINEX) 3.02 format to support the joint processing of multi-constellation and multi-frequency observations from GPS, BDS, GLONASS, and Galileo. Multi-GNSS precise orbit products released by CODE were used to calculate satellite elevation and azimuth angles for each epoch. Gauge water level data were employed to evaluate GNSS-IR retrieval accuracy, while ERA5 precipitation data were used to assist in the interpretation of the hydro-meteorological background and dynamic response relationship between the Huayuankou and Xiaolangdi stations.

During preprocessing, SNR observations were first extracted from the raw GNSS files, and satellite elevation and azimuth angles were computed using precise ephemerides to establish the basic observation sequences for subsequent screening and retrieval. Because GNSS-IR interference oscillations are more pronounced at low elevation angles with receiving surface reflected signals, the effective elevation-angle range was restricted to 5–15°. In addition, azimuth masks were defined according to local topographic conditions and the effective water reflection zones at the two sites. For Huayuankou, the azimuth ranges were set to 0–70° and 280–360°, whereas for Xiaolangdi, the azimuth range was set to 80–250°. After this spatial filtering, the retained SNR sequences were used as the effective observations for subsequent high-frequency water level retrieval.

2.2. High-Frequency GNSS-IR Water Level Retrieval

2.2.1. Data Preprocessing and Retrieval Methods

GNSS-IR retrieves the reflector height by analyzing the interference oscillation formed by the superposition of direct and water surface-reflected signals in receiver *SNR* observations. Raw SNR data are usually output in dB-Hz. To facilitate extraction of multipath interference oscillation features, they must first be converted into linear values. Let the observation be $SNR_{dB\text{-}Hz}$, and its linearized expression is

$$SNR_{lin} = 10^{SNR_{dB\text{-}Hz}/20} \tag{1}$$

where SNR_{lin} denotes the *SNR* series in linear form.

The geometric model of GNSS-IR water surface reflection is shown in Figure 3. When only a single specular reflection is considered, the geometric delay D of the reflected signal relative to the direct signal can be expressed as [21]

$$D = 2h \sin\theta \tag{2}$$

where h is the vertical distance from the receiver antenna phase center to the still water surface and θ is the instantaneous satellite elevation angle. According to the interference geometry of GNSS-IR, the residual oscillatory term can be written as [21]

$$\delta SNR = A \cos\left(\frac{4\pi h}{\lambda} \sin\theta + \phi\right) \tag{3}$$

where A is the composite amplitude of the oscillatory signal, λ is the wavelength of the corresponding GNSS carrier signal, and ϕ is the phase offset. Taking sinθ as the independent variable, the relationship between the dominant oscillation frequency f and the reflector height h can be obtained as [21]

$$h = \frac{f\lambda}{2} \tag{4}$$

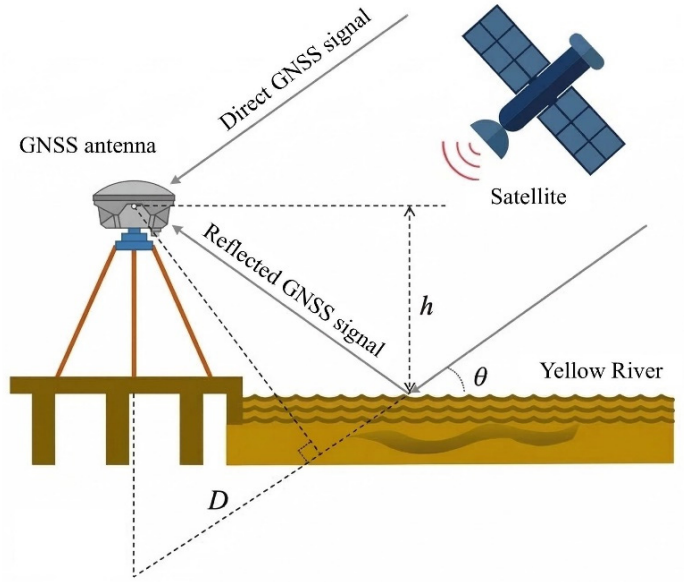


Figure 3. Geometric diagram of GNSS-IR water surface reflection.

Furthermore, if the elevation of the GNSS receiver antenna phase center under a unified elevation datum is H_{ant}, the final retrieved actual water surface elevation H_{water} can be expressed as

$$H_{water} = H_{ant} - h \quad (5)$$

The above equations constitute the geometric relation for GNSS-IR water level retrieval. The core idea is to retrieve reflector height and actual water surface elevation by extracting the dominant oscillation frequency of the δSNR series. In practical processing, the Lomb–Scargle spectral analysis method is used to extract the dominant frequency under uneven sampling, and Equations (4) and (5) are then used to compute the high-frequency water level results.

2.2.2. Sliding-Window High-Frequency Resampling Strategy

Unlike traditional approaches based on complete satellite arcs, this study introduces a sliding-window strategy into the GNSS-IR framework to improve the temporal resolution of water level retrieval. Traditional GNSS-IR methods typically treat a complete satellite pass lasting several hours as a single processing unit, meaning that each retrieval result represents an average condition over a relatively long time span and cannot adequately resolve short-term water level fluctuations under complex Yellow River hydrological conditions. To achieve high-frequency monitoring, a sliding-window strategy was adopted. The choice of a 40-minute window length is not arbitrary but is based on recent successful applications in highly dynamic water environments [8,26]. Previous studies have demonstrated that a 40-minute window provides an optimal balance: it covers a sufficient satellite elevation arc to capture enough multipath interference fringes for reliable Lomb–Scargle periodogram analysis while remaining short enough to prevent the over-smoothing of rapid water level fluctuations. In this study, a 40-minute window length and a 5-minute step size were adopted to segment the continuous SNR series locally and resample them densely, thereby transforming originally low-frequency and discrete retrievals into a continuous water level series with a 5-minute interval.

After window segmentation, additional quality control was applied to ensure the reliability of spectral analysis. Ascending and descending satellite arcs were processed separately to avoid spectral divergence caused by mixed reflection geometries. Observation segments with insufficient valid duration were removed to ensure adequate frequency res-

olution in the Lomb–Scargle analysis. Through this procedure, conventional low-frequency arc-based observations were reconstructed into dense and standardized short-time window sequences, providing the basis for subsequent VMD detrending, dominant-frequency extraction, and multi-GNSS joint estimation.

For clarity, the key parameter settings used in the high-frequency processing were as follows: an elevation-angle range of 5–15°, azimuth masks of 0–70° and 280–360° for Huayuankou, an azimuth mask of 80–250° for Xiaolangdi, a sliding-window length of 40 minutes, a sliding step of 5 minutes, and a minimum valid data length of 300 s. Together, these settings ensured stable reflection geometry and reliable spectral estimation within each short time window.

Overall, based on the above data screening and processing procedures, the key parameter settings involved in GNSS-IR water level retrieval are summarized in Table 1.

Table 1. Key preprocessing parameters for GNSS-IR water level retrieval.

Parameter	Value	Description
Elevation angle	5–15°	Reduce the influence of direct signals and enhance interference features
Huayuankou azimuth range	0–70° & 280–360°	Ensure that reflected signals come from a stable water surface
Xiaolangdi azimuth range	80–250°	Ensure that reflected signals come from a stable water surface
Sliding-window length	40 minutes	Ensure the frequency resolution of spectral analysis
Sliding step	5 minutes	Improve the temporal resolution of water level retrieval
Minimum data length	300 s	Ensure the stable extraction of interference periods

2.2.3. VMD Detrending and Dominant-Frequency Extraction

In GNSS-IR water level retrieval, the low-frequency trend is removed from the SNR series, which is a crucial step for isolating the effective reflected oscillation signal. Because SNR observations are formed by the superposition of direct and reflected signals, the direct component usually dominates the signal energy and appears as a slowly varying low-frequency trend with satellite elevation angle. If this trend is not removed, it can mask the multipath interference oscillations caused by water-surface reflection and degrade the accuracy of subsequent dominant-frequency extraction and water level retrieval.

Traditional methods usually fit the SNR sequence with a quadratic polynomial to characterize the overall trend and extract the residual sequence. The trend term can be expressed as

$$T(t) = a_0 + a_1 t + a_2 t^2 \tag{6}$$

where a_0, a_1, and a_2 are polynomial coefficients to be estimated. After detrending, the residual sequence can be written as

$$dSNR(t_i) = SNR(t_i) - T(t_i) \tag{7}$$

However, in the wide-shallow wandering reaches and canyon-controlled environments of the Yellow River, SNR sequences often contain obvious nonstationary noise because of shoals, vegetation, mountains, and variations in water surface roughness. A simple quadratic polynomial fit cannot simultaneously achieve effective trend removal and noise suppression. To improve the stability of high-frequency retrieval in complex environments, this study adopted VMD to detrend the SNR sequence. VMD can adaptively decompose the original signal into several modal components with different center frequencies and finite bandwidths, and its constrained variational model is expressed as [8]

$$\min_{\{u_k\},\{\omega_k\}} \left\{ \sum_{k=1}^{K} \| \partial_t \left[\left(\delta(t) + \frac{j}{\pi t} \right) * u_k(t) \right] e^{-j\omega_k t} \|_2^2 \right\}, \text{s.t.} \sum_{k=1}^{K} u_k(t) = x(t) \tag{8}$$

where $\{u_k\}_{k=1}^{K}$ denotes the K decomposed modal components and $\{\omega_k\}_{k=1}^{K}$ denotes the center frequency corresponding to each mode. Compared with the traditional quadratic polynomial fit, VMD is more adaptable for handling complex nonstationary multipath interference and can provide more stable input data for the subsequent Lomb–Scargle dominant-frequency extraction.

In practical GNSS-IR data processing, the VMD algorithm employs the Alternating Direction Method of Multipliers (ADMM) to alternately update the mode functions u_k and center frequencies ω_k until the objective function converges and the iteration stopping criteria are met. When applying the VMD method for SNR sequence detrending, the number of decomposition modes K must be predetermined. In this study, the number of VMD decomposition modes was fixed at $K = 5$ to ensure the effective separation of the direct-signal trend, the reflected-signal oscillations, and high-frequency noise. Figure 4 illustrates an example of VMD decomposition within a specific observation window at the Huayuankou station with the setting of $K = 5$. A comparison between the waveforms of the individual intrinsic mode function (IMF) components and the original SNR sequence reveals that the variation trend of IMF5 closely matched the low-frequency envelope of the SNR, representing the trend term induced by the direct signal. Conversely, IMF1 through IMF4 exhibited periodic oscillations, reflecting the characteristics of the water surface-reflected signal. Therefore, by discarding IMF5 along with any residual components and reconstructing IMF1 through IMF4, a high-quality SNR residual sequence, $dSNR$, can be obtained for subsequent water level retrieval.

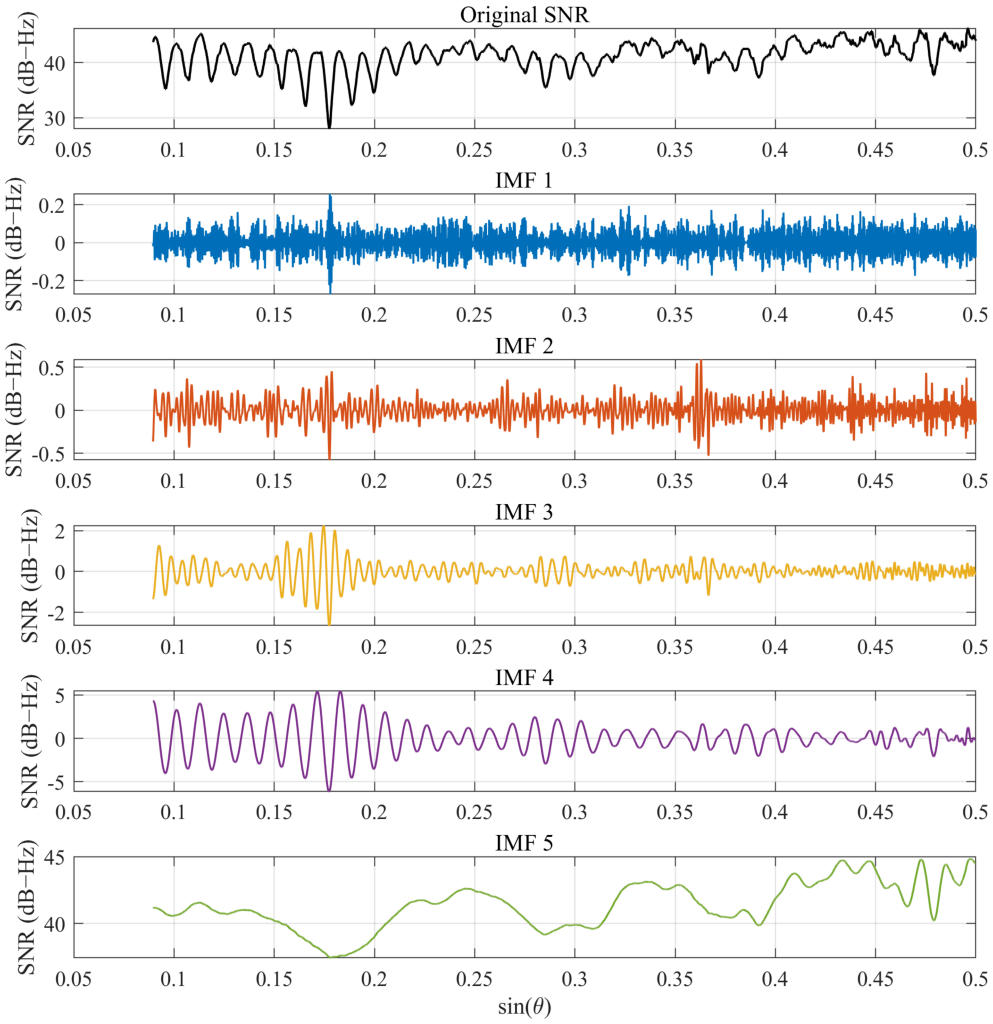


Figure 4. Original SNR signal and its IMF components obtained through VMD.

To visually demonstrate the practical performance of different trend separation strategies in complex hydrological environments, this study selected measured SNR data from a specific observation window at the Huayuankou station. Quadratic fitting (QF) and the VMD algorithm were separately applied for detrending, and a comparison of the extracted residual sequences is presented in Figure 5.

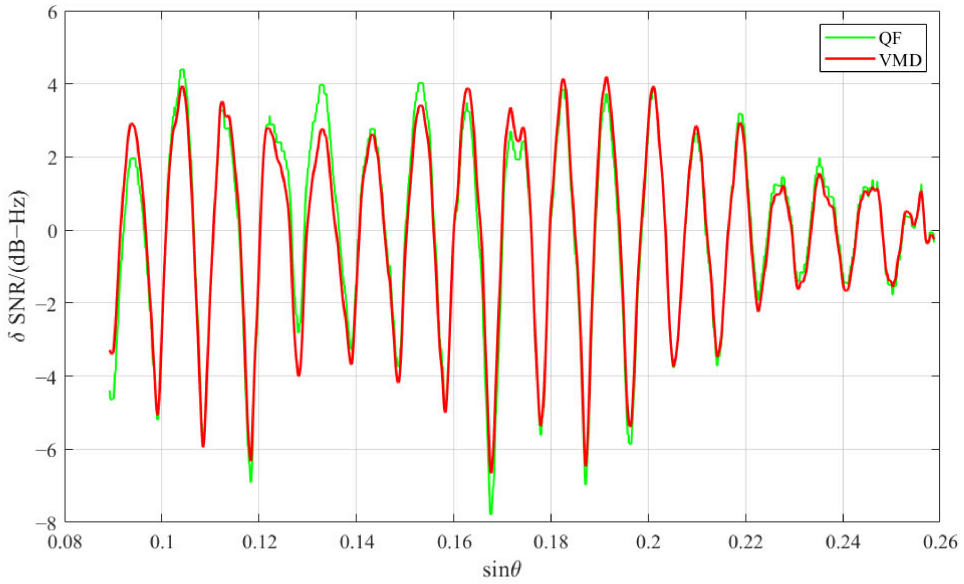


Figure 5. Effectiveness of QF and VMD in extracting $dSNR$.

The comparison between quadratic-polynomial fitting and VMD-processed dSNR shown in Figure 5 also indicates that the waveform after VMD detrending is smoother and more regular, which is more favorable for the stable identification of the dominant frequency.

Therefore, the long-term high-frequency water level series estimated in this study all adopt the processing route of 'sliding-window clipping + VMD detrending + Lomb–Scargle dominant-frequency extraction' to ensure the reliability and consistency of short-term retrieval results in complex river environments.

2.2.4. Multi-GNSS Joint Estimation

The integration of the sliding window, VMD, and multi-GNSS joint estimation forms a unified processing chain. Mathematically, the sliding window acts as a temporal operator that segments the continuous SNR series into localized units, ensuring the stationarity required for spectral analysis. Within each segment, VMD functions as a signal-processing operator that adaptively extracts the multipath oscillatory component for each signal track. Finally, the multi-GNSS joint estimation serves as the statistical integrator, which aggregates the retrieved water level estimates (derived from the dominant frequencies of these oscillations) across diverse GNSS constellations into a single, robust high-frequency water level series. This framework allows each step to reinforce the next: local segmentation (sliding window) provides the input for localized noise removal (VMD), which in turn yields reliable water level observations for the final robust statistical estimation (multi-GNSS joint estimation).

In high-frequency GNSS-IR retrieval, results from a single constellation or a single frequency are easily affected by local environmental noise, satellite geometry, and short-term observation condition changes, resulting in local discontinuities or fluctuations in accuracy. To improve the stability and continuity of high-frequency monitoring results, this study further adopts a multi-GNSS joint estimation strategy, incorporating valid

observations from BDS, GPS, GLONASS, and Galileo into a unified solution framework to jointly estimate the water level at the target epoch within a short time window.

Within a short time window, water level variation around the target epoch can be regarded as relatively stable. Therefore, valid retrieval results obtained from spectral analysis within this period can be jointly solved as observations of the same time interval. Let the observation vector be L, the design matrix be A, and the weight matrix be P; then the least-squares estimate of the multi-GNSS joint solution can be expressed as [26]

$$\hat{h} = (A^T PA)^{-1} A^T PL \tag{9}$$

where $\hat{h}$ is the water level estimate at the target epoch. Under the short-time static assumption adopted in this study, this model essentially reflects the joint estimation of the same target water level using multi-source observations.

To compensate for the possible insufficiency of valid satellites at a single epoch in the sliding-window step solution, valid retrieval results within a certain time range before and after the target epoch were incorporated into the current computation pool, and a dual initial weighting scheme jointly determined by signal quality and time-decay weighting was constructed as

$$P_{init} = W_{SNR} \cdot W_{Time} \tag{10}$$

where W_{SNR} is the peak SNR extracted during retrieval and characterizes the quality of the signal itself and W_{Time} is a time-decay weight based on a Gaussian distribution:

$$W_{Time} = \exp\left[-\left(\frac{\Delta t}{\sigma}\right)^2\right] \tag{11}$$

where Δt is the time difference between a neighboring observation and the target epoch, and σ is the Gaussian constant controlling the decay rate of the time weight. The further the observation is from the target epoch, the smaller its weight in the adjustment is, thereby increasing observational redundancy while avoiding time-lag effects.

In the complex multi-GNSS and multi-frequency observation environment, it is inevitable that some gross-error observations disturbed by abnormal water surface fluctuations or severe multipath effects will be mixed in. To prevent these outliers from biasing the least-squares optimum, the Institute of Geodesy and Geophysics (IGG) III scheme was used to dynamically update the weight matrix [27]. Let the standardized residual at the m iteration be v_s, then the equivalent weight $P^{(\mathrm{m})}$ is updated as

$$P^{(m)} = \begin{cases} P^{(m-1)}, |v_s| \le k_0 \\ P^{(m-1)} \frac{k_0}{|v_s|}\left(\frac{k_1 - |v_s|}{k_1 - k_0}\right)^2, k_0 < |v_s| \le k_1 \\ 0, |v_s| > k_1 \end{cases} \tag{12}$$

where k_0 and k_1 are discrimination thresholds. Observations with small standardized residuals retain their original weights, those between the thresholds are down-weighted, and those with excessively large residuals are removed from the adjustment model. Through repeated iterations until the water level change converges, a high-frequency water level series that is not significantly disturbed by extreme outliers can be obtained.

Figure 6 illustrates the overall workflow of the proposed GNSS-IR water level retrieval method. First, the SNR data is extracted from the GNSS raw observation files with the assistance of navigation files. The continuous SNR time series then undergoes windowing, detrending (to separate the direct signal component), and spectral analysis using the LSP (Lomb–Scargle Periodogram) method to determine the dominant frequencies. Subsequently,

the individual retrievals are fed into the GNSS-IR combined algorithm to generate a high-frequency, multi-GNSS fused water level series. Finally, an accuracy evaluation is performed by comparing the retrievals against the measured water level data to output the final results.

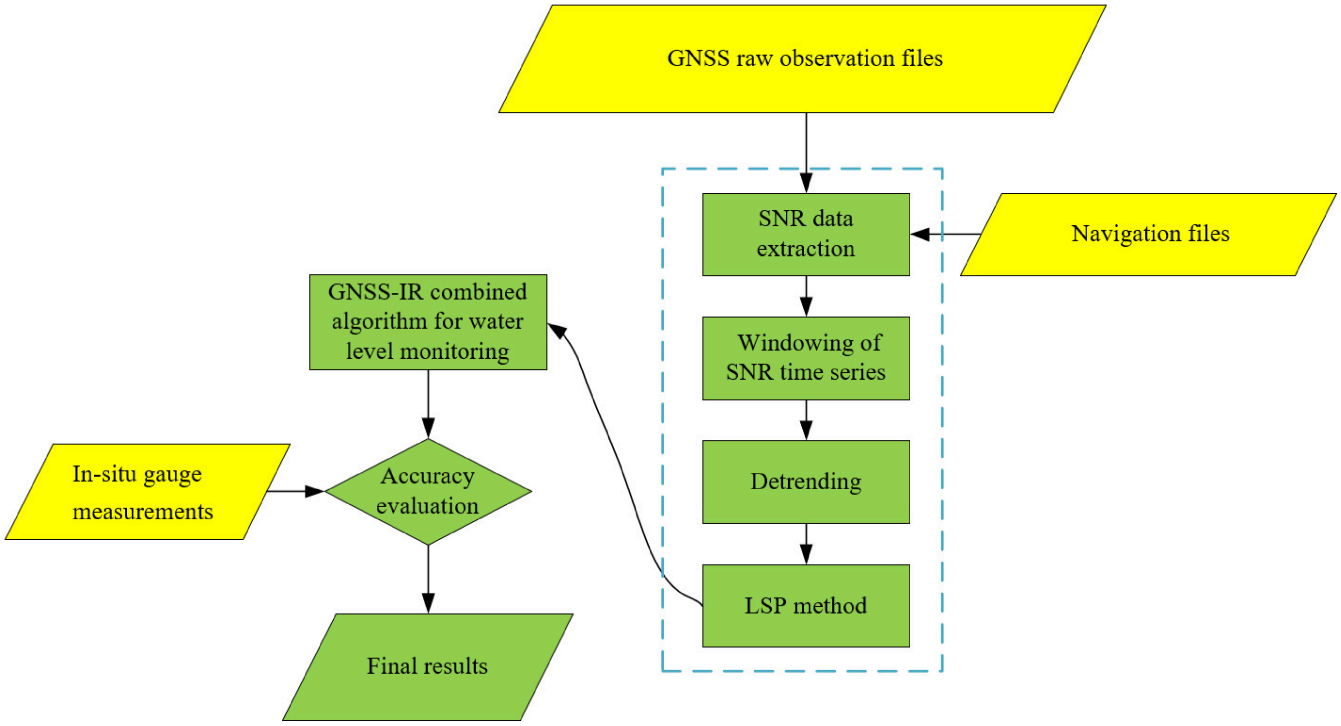


Figure 6. GNSS-IR water level retrieval process.

3. Results and Analysis

3.1. High-Frequency Water Level at Huayuankou

To evaluate the robustness of the proposed high-frequency GNSS-IR retrieval framework in a complex reflection environment, data collected at the Huayuankou station during day of year (DOY) 193–224 were processed.

Figure 7 shows the daily number of valid retrievals for different SNR types at Huayuankou during DOY 193–224. The overall trend indicates that the introduction of a 40-minute sliding window with a 5-minute step substantially increased the number of valid daily retrievals for all GNSS constellations. Over the 32-day study period, the total number of daily valid retrievals from GPS generally remained between 200 and 300, and it even exceeded 500 on specific days such as DOY 222. Meanwhile, the daily totals for BDS, GLONASS, and Galileo were mostly maintained within the range of 150–250. Compared with the conventional full-arc strategy, which typically yields only a limited number of discrete retrievals per day, the sliding-window approach greatly improved temporal coverage and provided a much denser basis for capturing short-term water level fluctuations in the Yellow River.

Under the combined effects of VMD-based detrending and quality control, different SNR types showed distinct levels of robustness in the wide-and-shallow river environment. In the GPS constellation, S1C was the most stable and productive signal type, consistently contributing more than 100 valid retrievals per day and thus serving as the main contributor to high-frequency GPS-based water level monitoring. The S2W and S5Q signals provided useful supplementary information, whereas S2X produced very few valid retrievals, indicating that this signal type was more susceptible to multipath contamination associated with surface roughness and therefore less reliable for high-frequency retrieval in this set-

ting. For BDS, S1I and S6I exhibited the highest availability and strongest consistency, whereas S7I showed very limited usability. In GLONASS, S1C consistently outperformed S2P, although all GLONASS signals experienced a sharp decline near DOY 209, most likely because of missing observations or severe local interference during that period. The Galileo constellation showed relatively larger day-to-day fluctuations, but S1C remained the most reliable signal type, followed by S7Q and S5Q.

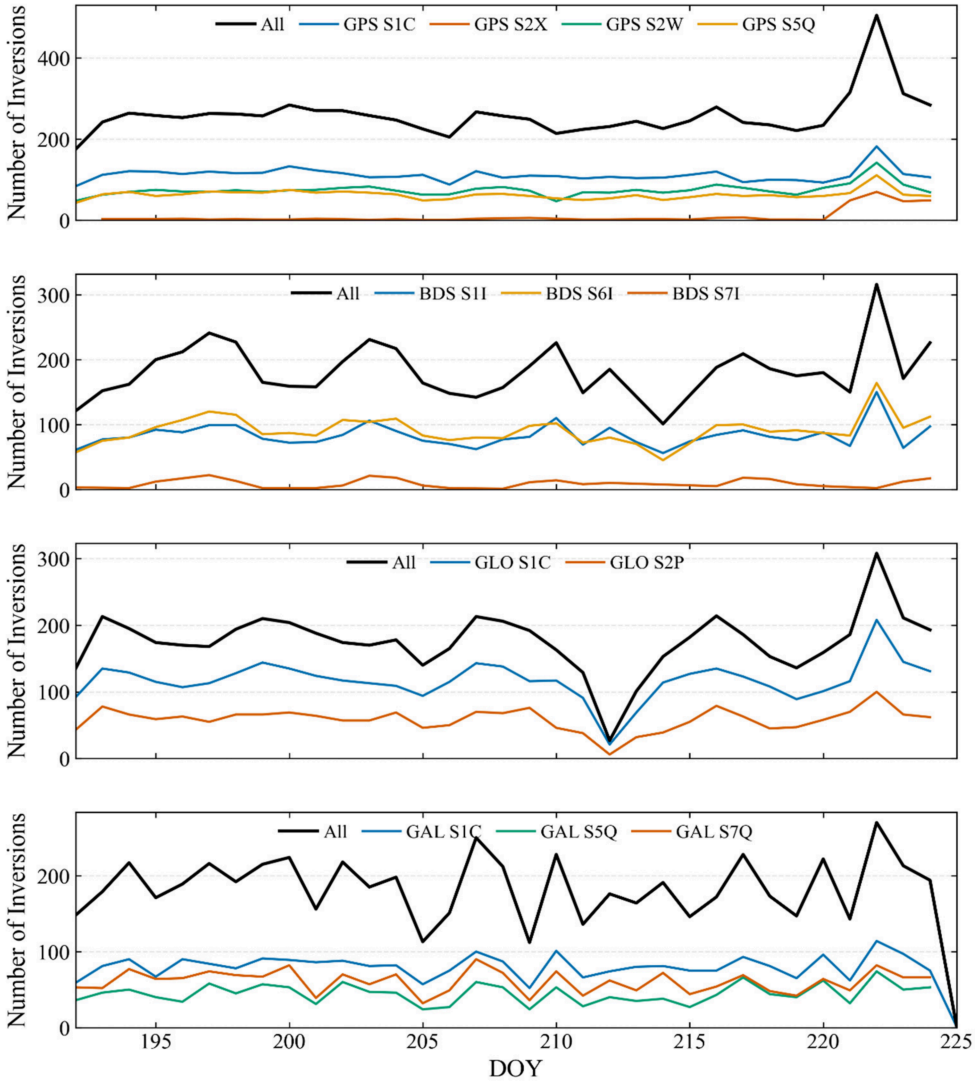


Figure 7. Daily valid retrieval counts of different SNR types at the Huayuankou station.

To quantify the improvement in retrieval density, Figure 8 compares the number of valid retrievals obtained from the conventional full-arc method and the high-frequency sliding-window strategy. The results show that the number of valid retrievals for the major signal types increased by approximately four to five times after high-frequency processing. For example, the number of valid retrievals for GLONASS-S1C increased from 685 to 3724, while that of GPS-S1C increased from 658 to 3574. This demonstrates that the sliding-window strategy not only increased the final number of retrievals but also made more effective use of the original GNSS observations for high-frequency water level monitoring. This information is available in the Supplementary Material (see Table S1).

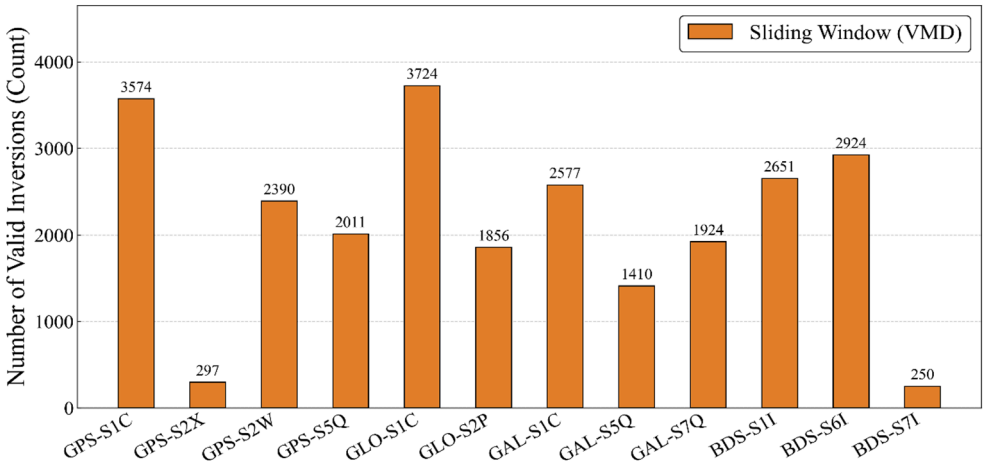


Figure 8. Number of retrieval results after applying the sliding window.

To further evaluate retrieval performance under multi-constellation and multi-frequency conditions, all valid high-frequency retrievals during DOY 193–224 were statistically assessed against gauge observations. Table 2 lists the number of valid samples, RMSE, and correlation coefficients for the principal signal types of the four GNSS constellations. Figures 9 and 10 present the corresponding water level time series and correlation analyses. Among the 12 tested signal types, most achieved an RMSE below 0.15 m and a correlation coefficient above 0.90, indicating that the proposed framework maintained good retrieval performance even under the highly complex multipath conditions of the wide-and-shallow Yellow River reach. Only a few signal types, such as GLONASS-S2P and Galileo-S5Q, showed weaker performance, with RMSE values slightly above 0.16 m and correlation coefficients below 0.87. These results suggest that VMD can effectively suppress nonstationary noise and support stable dominant-frequency extraction in this challenging environment.

However, good nominal accuracy does not necessarily imply practical usefulness. For example, although GPS-S2X and BDS-S7I yielded relatively low RMSE values of 0.088 m and 0.116 m, respectively, the total number of valid samples dropped sharply to only 297 and 250. Such severe data scarcity indicates that these signal types were highly vulnerable to environmental noise and could not provide sufficiently continuous support for high-frequency water level monitoring. Therefore, despite their apparently acceptable numerical accuracy in a small number of retained samples, they are not suitable as primary signal types for operational retrieval in this river setting.

Table 2. Valid retrieval counts, RMSE, and R for different SNR types.

SNR Type	Count	RMSE (m)	R
GPS-S1C	3574	0.142	0.916
GPS-S2X	297	0.088	0.890
GPS-S2W	2390	0.114	0.946
GPS-S5Q	2011	0.186	0.842
GLONASS-S1C	3724	0.106	0.931
GLONASS-S2P	1856	0.165	0.844
Galileo-S1C	2577	0.158	0.869
Galileo-S5Q	1410	0.162	0.860
Galileo-S7Q	1924	0.129	0.913
BDS-S1I	2651	0.137	0.890
BDS-S6I	2924	0.097	0.936
BDS-S7I	250	0.116	0.909

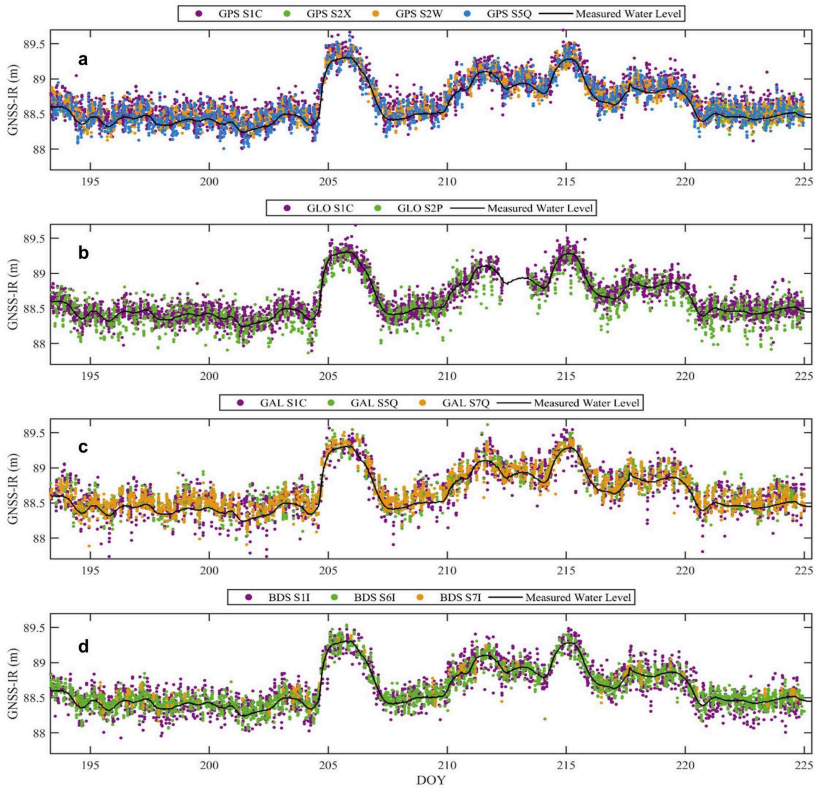


Figure 9. GNSS-IR water level retrieval results: GPS (**a**), GLONASS (**b**), Galileo (**c**), and BDS (**d**).

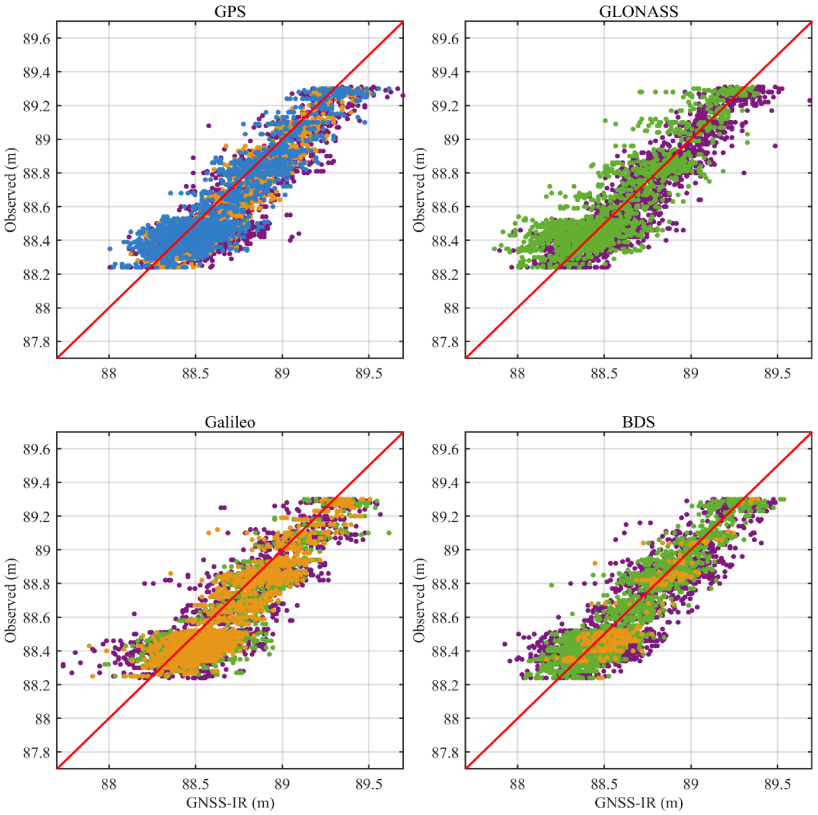


Figure 10. Correlation analysis of high-frequency retrieval results for single-system, single-frequency bands at the Huayuankou station. The red solid line represents the 1:1 reference line (y = x). Scatter points in different colors denote different frequency bands within each constellation (Purple: GPS S1C, GLO S1C, GAL S1C, and BDS S1I; Green: GPS S2X, GLO S2P, GAL S5Q, and BDS S6I; Orange: GPS S2W, GAL S7Q, and BDS S7I; Blue: GPS S5Q).

Building on the single-frequency analysis, multi-frequency fusion was further performed within each GNSS constellation. The results in Figure 10 and Table 3 show that the fused time series of each constellation tracked the observed water level variations more continuously than individual signal types. Among them, BDS achieved the best overall performance, with an RMSE of 9.9 cm and an R^2 of 0.937, indicating that multi-frequency complementarity improved the continuity and stability of single-constellation retrievals. This information is available in the Supplementary Material (see Table S2). On this basis, the multi-GNSS combined results obtained using quadratic fitting (QF) and VMD as detrending methods were further compared. Although both methods produced continuous high-frequency water level retrievals over the study period, VMD yielded better accuracy, reducing the RMSE from 9.7 cm to 8.6 cm. This indicates that VMD is more suitable than conventional quadratic fitting for constructing the final long-term high-frequency water level series at Huayuankou.

Table 3. Comparison of multi-GNSS combinations using QF and VMD methods.

Method	Number of Results	RMSE (cm)	R^2
QF	8089	9.7	0.924
VMD	7925	8.6	0.921

Based on the above analyses, the final long-term high-frequency water level series at Huayuankou was constructed using the sliding-window, VMD, and multi-GNSS joint-estimation framework. The combined solution produced 7925 valid water level estimates, with an RMSE of 0.086 m and an R^2 of 0.921 over the full study period. These results demonstrate that the proposed method can simultaneously achieve high temporal resolution, good continuity, and high accuracy in a wide-and-shallow wandering river reach.

3.2. High-Frequency Water Level at Xiaolangdi

To further verify the applicability of the proposed method under strongly dynamic river conditions, the same processing strategy was applied to the Xiaolangdi station during the period from 1 May to 31 August 2025.

Using the period from 1 May to 31 August 2025 as the study interval, the multi-GNSS high-frequency GNSS-IR retrievals showed good agreement with the observed water level series at Xiaolangdi. As illustrated in Figure 11, the retrieved time series reproduced the overall pattern of water level variation throughout the study period. The retrievals matched the gauge observations closely during relatively stable periods and were still able to continuously track rapid changes during rising and falling stages without obvious interruptions or large deviations.

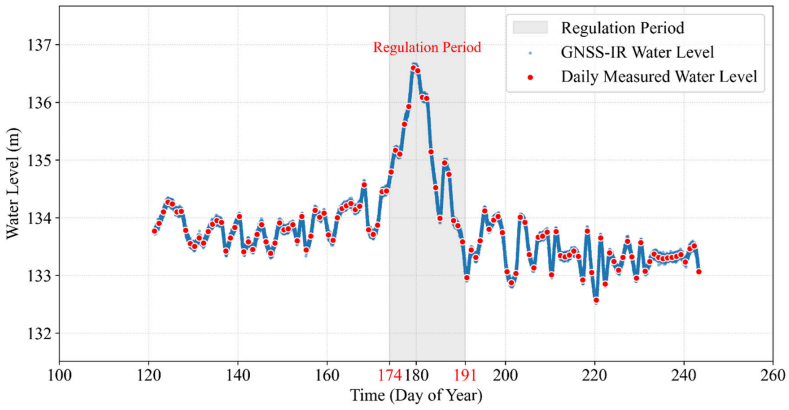


Figure 11. Comparison between GNSS-IR and measured water levels at the Xiaolangdi station.

Statistical evaluation indicates that the retrieved water levels at Xiaolangdi achieved an R^2 of 0.963 and an RMSE of 0.138 m, demonstrating that the final method maintained high retrieval accuracy even under canyon terrain and strong reservoir-regulation forcing. Compared with Huayuankou, the Xiaolangdi reach is jointly influenced by canyon topography, reservoir operation, and local reflection-boundary conditions, and its water level process therefore exhibits a more concentrated regulation signal. The good performance obtained at Xiaolangdi suggests that the proposed method is applicable not only to wide-and-shallow wandering channels, but also to canyon-controlled river sections strongly affected by engineering regulation.

From the perspective of process representation, the high-frequency retrieval series at Xiaolangdi captured not only slow water level variations during relatively stable periods, but also rapid stage changes during water and sediment regulation operation. During the period of intensified reservoir regulation, the rate of water level change increased substantially, yet the retrieved series remained continuous overall. This indicates that the final method has good stability and timeliness under strongly dynamic conditions. Compared with low-frequency discrete observations, the high-frequency series provided much finer details of temporal variation, thereby establishing a solid basis for identifying stage-dependent dynamic responses during the regulation process.

3.3. Long-Term High-Frequency Water Level

Based on the high-frequency retrieval results at Huayuankou and Xiaolangdi, this study further constructed a two-station long-term high-frequency water level dataset for dynamic process analysis. The Huayuankou series primarily reflects water level evolution in the downstream wide-and-shallow wandering reach, whereas the Xiaolangdi series mainly captures the concentrated upstream response associated with reservoir regulation in the canyon-controlled reach. Together, the two stations form a clear upstream–downstream pair, and the use of a unified high-frequency GNSS-IR framework ensures that the resulting time series are continuous and directly comparable, thereby providing a consistent basis for the subsequent analysis of dynamic response during water and sediment regulation.

Overall, the two-station high-frequency series constructed using the same final method maintained good accuracy and continuity at both sites. The results at Huayuankou show that the method can adapt to the complex non-water diffuse-reflection background of a wide-and-shallow wandering channel, while the results at Xiaolangdi show that it can remain stable in a canyon reach characterized by strong regulation effects and rapid water level changes. The key advantage of this unified two-station framework is that subsequent dynamic process analysis no longer depends on data from different sources, different temporal resolutions, or different processing strategies, but instead relies on continuous water level series derived from the same GNSS-IR methodology, thereby improving both consistency and interpretability.

Figure 12 presents the high-frequency water level response of the Xiaolangdi and Huayuankou stations during the 2025 water and sediment regulation operation, and Table 4 summarizes the key parameters of flood wave propagation. The results show that the flood peak at Xiaolangdi occurred at 15:00 on 28 June 2025, with a peak water level of 136.60 m, whereas the corresponding peak at Huayuankou occurred at 12:00 on 29 June 2025, with a peak water level of 90.70 m. The difference in peak timing between the upstream and downstream stations was therefore about 21 h. These results indicate that the two-station long-term high-frequency series can clearly support the identification of dynamic response and flood wave propagation during the water and sediment regulation process.

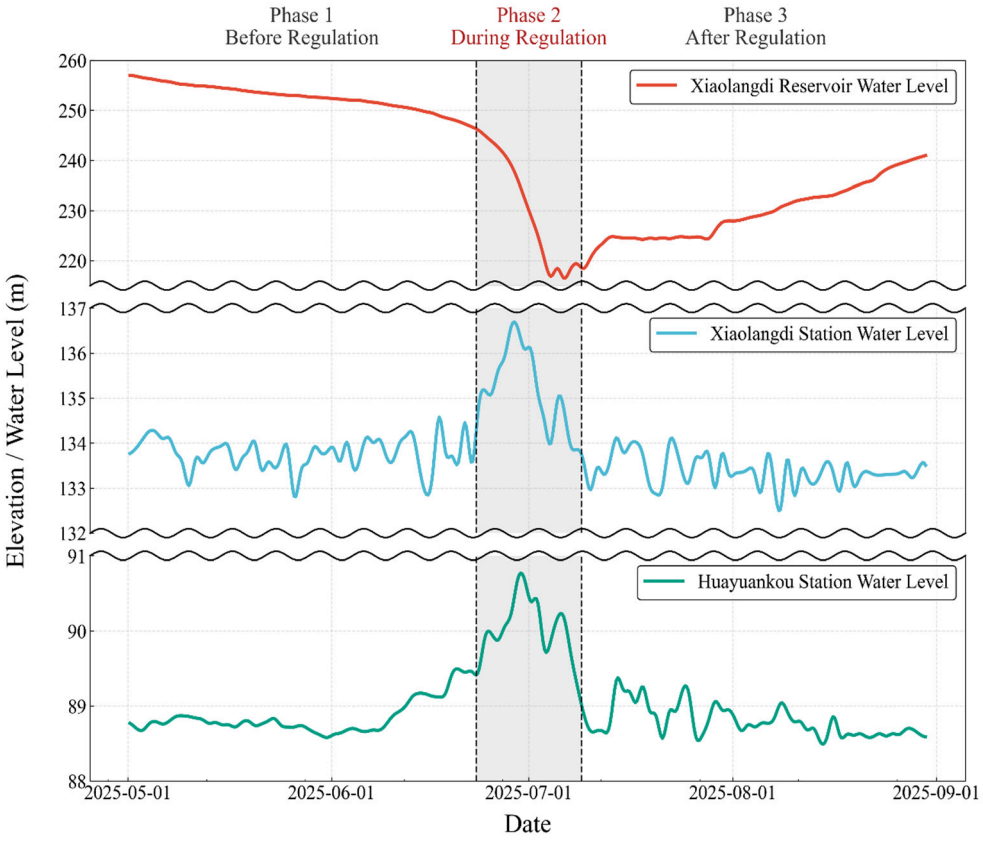


Figure 12. Water level response processes at the Xiaolangdi and Huayuankou stations during water-sediment regulation.

Table 4. Statistics of key parameters for typical flood wave propagation.

Station/Indicator	Time of Peak Occurrence	Peak Water Level/m	Process Characteristics
Xiaolangdi	28 June 2025 15:00	136.60	Rapid response, sharp peak
Huayuankou	29 June 2025 12:00	90.70	Lagged response, broader peak top

3.4. Water Level Responses to Water-Sediment Regulation at Xiaolangdi

To further assess the applicability of the high-frequency GNSS-IR water- level series for monitoring complex hydrological processes, this section focuses on the Xiaolangdi station and examines its water level response during a representative water and sediment regulation event in 2025. Xiaolangdi is located near the outlet of the last canyon reach in the middle Yellow River and serves as a key control node for flood regulation and water-sediment management in the middle and lower basin. Because its water level variations directly reflect upstream reservoir operation and release processes, it provides an ideal setting for evaluating the capability of high-frequency water level monitoring under strong anthropogenic forcing.

Figure 11 compares the GNSS-IR-retrieved water levels at Xiaolangdi with the corresponding gauge observations. The retrieved series captures the overall pattern of water level variation well throughout the study period. During relatively stable stages, the retrievals remained highly consistent with the observed water levels, whereas during rapidly rising or falling stages, the series still continuously tracked the temporal evolution without obvious discontinuities or large deviations. These results indicate that the high-frequency series generated from the sliding-window, VMD, and multi-GNSS joint-estimation framework can reliably represent the water level dynamics at Xiaolangdi under complex and strongly varying conditions.

The 30th Yellow River water and sediment regulation operation in 2025 was initiated on 23 June and lasted for approximately 17 days. During this period, Xiaolangdi Reservoir released a relatively large discharge to create storage capacity for flood control and to enhance downstream channel flushing, causing a pronounced rise in river stage within a short time. The high-frequency water level series shows that the Xiaolangdi station responded rapidly after the onset of regulation, shifting from a relatively stable pre-event state to a clear rising stage and eventually forming a concentrated artificial flood peak during the core regulation period. This indicates that the water level variations at Xiaolangdi were directly and sensitively controlled by upstream reservoir operations.

In terms of hydrograph shape, the Xiaolangdi series exhibited a rapid rise, concentrated peak formation, and relatively rapid recession, producing a distinctly sharp flood peak. This behavior is consistent with the hydraulic setting of a canyon-controlled reach, where channel boundaries are relatively confined and the regulation signal from reservoir releases is strongly expressed. Compared with downstream wandering reaches, the local channel near Xiaolangdi provides less attenuation and storage effect, so its water level response is more direct and more representative of the upstream artificial regulation signal itself. Overall, the Xiaolangdi results demonstrate that the high-frequency GNSS-IR series can effectively record the rapid hydrological response during water and sediment regulation, thereby providing a reliable upstream boundary series for subsequent two-station dynamic response analysis.

3.5. Flood Wave Propagation and Evolution from Xiaolangdi to Huayuankou

After obtaining the high-frequency water level series at Xiaolangdi and Huayuankou, the flood wave propagation process along this key Yellow River reach was further analyzed under the water and sediment regulation scenario. The Xiaolangdi–Huayuankou reach extends approximately 115 km and is characterized by a typical wandering channel with a wide-and-shallow morphology and strong channel-storage capacity. When Xiaolangdi Reservoir releases a concentrated high discharge, the resulting flood wave is jointly influenced by channel resistance, reach-scale storage, and changing boundary conditions during downstream propagation, leading to pronounced evolution in both travel time and peak shape.

The observed ~21-h propagation lag of the flood peak from Xiaolangdi to Huayuankou (as detailed in Section 3.3) is primarily governed by the strong channel storage capacity of this wide-and-shallow wandering reach. Rather than a simple synchronous downstream transmission, the flood wave undergoes significant energy dissipation and spatial redistribution. This attenuation process not only reshapes the sharp artificial flood peak into a broader downstream hydrograph but also highlights the critical buffering role of the Xiaolangdi–Huayuankou channel during major water-sediment regulation operations.

In addition to the propagation delay, the flood peak morphology also changed markedly. Compared with the relatively sharp and concentrated flood peak at Xiaolangdi, the water level hydrograph at Huayuankou shows more gradual rising and falling limbs, a broader peak crest, and a longer peak duration. This indicates that the flood wave underwent pronounced flattening and attenuation during downstream propagation, as part of the peak energy was absorbed and redistributed by the wide-and-shallow channel and adjacent floodplain-like shoal areas. As a result, the originally steep and concentrated upstream peak evolved into a more dispersed and flattened downstream hydrograph.

A similar contrast was observed during the recession stage. After reservoir regulation weakened, the water level at Xiaolangdi declined relatively quickly, whereas the recession at Huayuankou was clearly delayed and exhibited a trailing effect. This suggests that water temporarily stored within the channel and along channel storage zones continued to

drain back into the main channel during the falling stage, thereby extending the overall response duration of the flood wave. The two-station high-frequency water level series therefore not only resolves the travel time difference of the flood peak but also captures the morphological transition from a sharp upstream peak to a broader and more attenuated downstream hydrograph.

4. Discussion

4.1. Meteorological and Stage-Wise Decoupling Characteristics

To further interpret the driving background of the high-frequency water level variations at the two stations, this study compared the water level series with meteorological conditions in the Xiaolangdi Reservoir area and the downstream river reach. Figure 13 illustrates the co-variation between the water level process and the hydro-meteorological background. At longer time scales, the regional hydro-meteorological conditions showed a certain degree of consistency, suggesting that the transitional zone between the middle and lower Yellow River is influenced by a relatively coherent external climatic background.

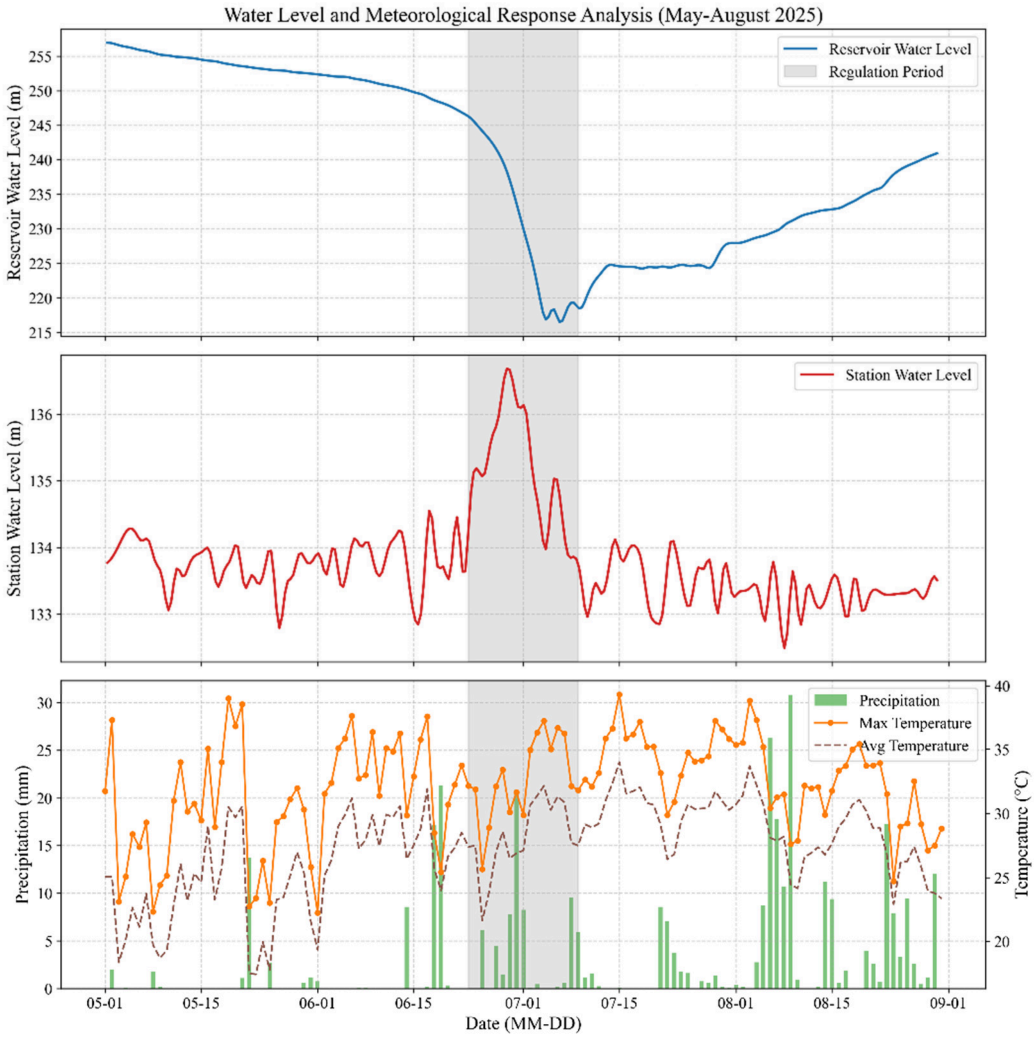


Figure 13. Coordinated variations of water levels and meteorological elements in the Xiaolangdi Reservoir and the downstream river channel.

However, during the 2025 water and sediment regulation event, short-term water level variations were not governed solely by local precipitation but instead exhibited a clear stage-dependent decoupling from meteorological forcing. Before the onset of the

regulation event, precipitation in the study area was limited and river stages fluctuated mainly within their normal range. During the core regulation period, by contrast, the downstream station experienced a rapid rise in water level and a distinct flood peak despite the absence of notable regional rainfall. This indicates that the dominant driver of water level change during this stage was not local precipitation, but rather the large-discharge artificial regulation released from Xiaolangdi Reservoir.

These results suggest that meteorological background alone is insufficient to explain water level variations during typical Yellow River regulation events. For the Xiaolangdi–Huayuankou reach, long-term hydro-meteorological coherence mainly reflects a shared regional background, whereas short-term high-frequency stage changes are more strongly controlled by reservoir regulation. In this sense, the construction of a two-station high-frequency water level dataset makes it possible to separate and analyze the respective roles of natural background conditions, engineering regulation, and channel response.

4.2. Impacts of Dynamic Responses and Possible Causes

The two-station high-frequency water level series from Xiaolangdi and Huayuankou shows that the water level response of this key Yellow River reach during water and sediment regulation was characterized by clear spatial heterogeneity and strong stage dependence. Xiaolangdi responded rapidly to concentrated upstream reservoir releases and was the first to form a distinct artificial flood peak, whereas Huayuankou exhibited a pronounced lagged response accompanied by attenuation, flattening, and trailing recession during downstream propagation. These differences indicate that the influence of water and sediment regulation is not transmitted downstream in a simple synchronous manner but is instead jointly modulated by multiple hydraulic and geomorphic factors during channel propagation.

Several factors may explain this behavior. First, the concentrated reservoir release from upstream was the direct trigger of the two-station dynamic response. After the regulation operation began, the water level at Xiaolangdi rose rapidly and formed a clear peak, indicating that its high-frequency stage process was primarily controlled by reservoir operation. Second, the Xiaolangdi–Huayuankou reach is a typical wide-and-shallow wandering channel with broad channel geometry, developed shoals, and substantial channel storage capacity. During downstream propagation, the flood wave was therefore prone to energy dissipation and storage effects, which in turn delayed the downstream peak, broadened the crest, and prolonged the recession stage. Third, factors such as channel resistance, along-reach boundary conditions, and local channel morphology likely further affected both propagation speed and hydrograph evolution, making the Huayuankou response the integrated result of upstream regulation forcing and downstream channel-adjustment effects.

From a practical perspective, these dynamic response differences imply that the key Yellow River reaches under water and sediment regulation exhibit clear process propagation and spatial asynchrony. The observed flood wave travel time of about 21 h provides a potentially useful lead time for downstream flood control deployment and emergency regulation, while the attenuation and flattening of the flood peak suggest that the wandering channel can play a buffering and redistributive role with respect to the upstream regulation signal. In this sense, the two-station high-frequency GNSS-IR series not only identified the response time difference between upstream and downstream stations, but also revealed the hydrological significance of channel storage and flood wave transformation during regulation events.

4.3. Applicability and Future Prospects

Taken together, the results from Huayuankou and Xiaolangdi indicate that the proposed high-frequency GNSS-IR water level retrieval method shows good applicability across different river environments. At Huayuankou, a typical wide-and-shallow wandering reach with complex channel boundaries and strong non-water reflections, the method still produced a continuous and stable water level series, demonstrating strong resistance to interference in complex reflection environments. At Xiaolangdi, a canyon-controlled reach strongly affected by reservoir operation, the method continuously tracked rapid water level variations, indicating good adaptability under highly dynamic hydrological conditions.

From an application perspective, the method offers the advantages of non-contact measurement, continuous observation, and direct reliance on existing GNSS reference stations, thereby avoiding the vulnerability of conventional water level gauges under conditions of high flow velocity and high sediment concentration. At the same time, the high-frequency retrieval results provide much finer information on water level variation, which is valuable for improving the timeliness of water level monitoring in complex river reaches and for supporting the identification of water and sediment regulation processes, upstream–downstream dynamic response analysis, and flood wave propagation studies.

Furthermore, a systematic comparison with satellite altimetry (e.g., Sentinel-3 or ICESat-2) highlights the unique spatial and temporal advantages of the proposed ground-based GNSS-IR method. While satellite altimetry provides valuable large-scale monitoring, its operational utility in inland rivers is severely restricted. Spatially, its large footprints often suffer from 'land contamination' in narrow channels or canyon-controlled reservoirs, requiring complex waveform retracking. Temporally, its long revisit cycles (27 to 91 days) make it inherently incapable of resolving short-term, event-driven phenomena, such as the 17-day water-sediment regulation process. In contrast, ground-based GNSS-IR bypasses these bottlenecks. Spatially, it requires only a highly localized First Fresnel Zone—extending from just a few meters to tens of meters from the antenna—which effectively avoids bank interference. Temporally, it delivers ultra-high resolution (5-minute interval) via sliding-window resampling. This combination allows the proposed framework to seamlessly capture transient flood waves and quantify exact propagation lags, offering critical algorithmic advantages for real-time risk assessment in highly regulated rivers.

Nevertheless, several limitations should also be acknowledged. First, adjacent windows in the sliding-window scheme overlap substantially, so the resulting high-frequency retrievals are temporally correlated to some extent, which may affect the statistical independence of subsequent analyses. Second, high-frequency GNSS-IR retrievals still depend on satellite visibility and reflection geometry, and the results may fluctuate during periods with less favorable observation conditions. Third, this study is based mainly on two representative stations, Huayuankou and Xiaolangdi, and the applicability of the conclusions to other types of water bodies remains to be further verified.

Overall, the proposed method exhibits good stability and applicability in the complex inland river environment of the Yellow River and shows clear potential for extending water level monitoring from conventional low-frequency discrete observations to high-frequency continuous measurements. However, broader applications of the method will still require further validation under different hydrological and geomorphological settings, together with continued refinement of quality control strategies and evaluation procedures.

Finally, assessing the economic and operational advantages of GNSS-IR requires a nuanced perspective. Deploying a new geodetic-grade GNSS setup specifically for water level monitoring may not offer a clear cost advantage over mature radar gauges. However, the true strength of GNSS-IR emerges in two specific scenarios. First, by leveraging existing GNSS stations (e.g., regional CORS networks) near riverbanks, high-frequency water level

data can be extracted as a highly cost-effective byproduct without additional hardware. Second, in multi-hazard environments, a single GNSS station offers a unique dual capability: simultaneously measuring water level variations via reflectometry and providing absolute 3D positioning to track the structural deformation of dams and riverbanks. This directly ties the water level to a stable global reference frame—a critical advantage traditional radar sensors lack.

5. Conclusions

To address the limitations of traditional GNSS-IR water level retrieval in temporal resolution and continuous monitoring under complex river conditions, this study developed a high-frequency retrieval framework based on a sliding window, VMD detrending, and multi-GNSS joint estimation at the Huayuankou and Xiaolangdi stations. The main conclusions are as follows:

(1) The proposed framework effectively improves the temporal resolution, continuity, and stability of GNSS-IR water level retrieval in complex inland rivers. Compared with the traditional full-arc method, it makes better use of short-time interference signals and provides a reliable basis for long-term high-frequency water level monitoring.

(2) At Huayuankou, the method achieved continuous and high temporal resolution water level estimation at a 5-minute interval with an RMSE of 0.086 m, and an R^2 of 0.921. At Xiaolangdi, the retrieved series also agreed well with gauge observations, with an RMSE of 0.138 m and an R^2 of 0.963. These results confirm the applicability of the method in both wide-and-shallow wandering channels and canyon-controlled reaches affected by reservoir regulation.

(3) The two-station high-frequency series clearly captured the dynamic response of the Yellow River during the 2025 water and sediment regulation operation. Xiaolangdi responded rapidly and formed the flood peak first, whereas Huayuankou showed a delayed response, with the peak arriving about 21 h later. During downstream propagation over about 115 km, the flood wave exhibited attenuation, flattening, and trailing recession. This demonstrates the value of high-frequency GNSS-IR observations for dynamic response analysis and flood wave propagation studies.

Supplementary Materials: The following supporting information can be downloaded at: https://www.mdpi.com/article/10.3390/rs18111812/s1, Table S1: Valid retrieval counts, RMSE, and R for different SNR types using the traditional full-arc method; Table S2: Accuracy comparison of multi-frequency combined retrievals within single constellations.

Author Contributions: Conceptualization, Y.F. and S.J.; methodology, S.J.; software, Y.F.; validation, Y.F., S.J. and L.H.; formal analysis, L.H.; investigation, Y.F.; resources, S.J.; data curation, Y.F.; writing—original draft preparation, L.H.; writing—review and editing, S.J.; visualization, L.H.; supervision, S.J.; project administration, S.J.; funding acquisition, S.J. All authors have read and agreed to the published version of the manuscript.

Funding: This work was supported by the Henan International Science and Technology Cooperation Key Program (Grant No. 241111520700).

Data Availability Statement: The original data presented in the study are included in the article, and further inquiries can be directed to the corresponding author.

Acknowledgments: Authors also thank the Xiaolangdi and Huayuankou hydrological stations for providing the water level data.

Conflicts of Interest: The authors declare no conflicts of interest.

Abbreviations

The following abbreviations are used in this manuscript:

BDS	BeiDou Navigation Satellite System
CODE	Center for Orbit Determination in Europe
DOY	Day of Year
ERA5	Fifth Generation of ECMWF Atmospheric Reanalysis
GLONASS	Global Navigation Satellite System
GNSS	Global Navigation Satellite System
GNSS-IR	Global Navigation Satellite System Interferometric Reflectometry
GPS	Global Positioning System
QF	Quadratic Fitting
RINEX	Receiver Independent Exchange Format
RMSE	Root Mean Square Error
SNR	Signal-to-Noise Ratio
VMD	Variational Mode Decomposition

References

1. Ma, F.; Ma, L.; Lou, B.; Ye, W.; Li, W. A seepage monitoring model for earth-rock dams considering the change rate of reservoir water level. *Hydro-Sci. Eng.* **2025**, *5*, 78–87. [CrossRef]
2. Xu, L.; Wang, Y.; Hua, X. Research on application of radar level meter in automatic water regime monitoring system. *Yangtze River* **2014**, *45*, 74–77. [CrossRef]
3. Guo, X.; Jin, S. Water level changes in the Three Gorges of the Yangtze River from ICESat-2 laser altimeter data. *Sci. Surv. Mapp.* **2022**, *47*, 21–26. [CrossRef]
4. Domeneghetti, A.; Molari, G.; Tourian, M.J.; Tarpanelli, A.; Behnia, S.; Moramarco, T.; Sneeuw, N.; Brath, A. Testing the use of single- and multi-mission satellite altimetry for the calibration of hydraulic models. *Adv. Water Resour.* **2021**, *151*, 103887. [CrossRef]
5. Jin, S.G.; Park, J.; Wang, J.; Choi, B.; Park, P. Electron density profiles derived from ground-based GPS observations. *J. Navig.* **2006**, *59*, 395–401. [CrossRef]
6. Jin, S.G.; Zhu, W.; Afraimovich, E. Co-seismic ionospheric and deformation signals on the 2008 magnitude 8.0 Wenchuan Earthquake from GPS observations. *Int. J. Remote Sens.* **2010**, *31*, 3535–3543. [CrossRef]
7. Martin-Neira, M.; Caparrini, M.; Font-Rossello, J.; Lannelongue, S.; Vallmitjana, C. The PARIS concept: An experimental demonstration of sea surface altimetry using GPS reflected signals. *IEEE Trans. Geosci. Remote Sens.* **2001**, *39*, 142–150. [CrossRef]
8. Jin, S.G.; Chen, Z.; Peng, H. High-frequency centimeter-accuracy water level estimation in the Yangtze River using multi-GNSS interferometric reflectometry. *IEEE Trans. Geosci. Remote Sens.* **2025**, *63*, 5802713. [CrossRef]
9. Wang, Y.; Xie, T.; Li, J.; Zhang, X.H.; Bai, S.Y.; Wang, M.H. Sea ice concentration retrieval using spaceborne GNSS-R during the melting period. *Haiyang Xuebao* **2024**, *46*, 127–136. [CrossRef]
10. Jin, S.G.; Feng, G.; Gleason, S. Remote sensing using GNSS signals: Current status and future directions. *Adv. Space Res.* **2011**, *47*, 1645–1653. [CrossRef]
11. Wu, X.; Jin, S.G. GNSS-Reflectometry: Forest canopies polarization scattering properties and modeling. *Adv. Space Res.* **2014**, *54*, 863–870. [CrossRef]
12. Bian, S.; Zhou, W.; Liu, L.; Li, H.; Liu, B. GNSS-IR model of snow depth estimation combining wavelet transform with sliding window. *Acta Geod. Cartogr. Sin.* **2020**, *49*, 1179–1188. [CrossRef]
13. Larson, K.M.; Gutmann, E.D.; Zavorotny, V.U.; Braun, J.J.; Williams, M.W.; Nievinski, F.G. Can we measure snow depth with GPS receivers? *Geophys. Res. Lett.* **2009**, *36*, L17502. [CrossRef]
14. Jin, S.G.; Camps, A.; Jia, Y.; Wang, F.; Martin-Neira, M.; Huang, F.; Yan, Q.; Zhang, S.; Li, Z.; Edokossi, K.; et al. Remote sensing and its applications using GNSS reflected signals: Advances and prospects. *Satell. Navig.* **2024**, *5*, 19. [CrossRef]
15. Larson, K.M.; Löfgren, J.S.; Haas, R. Coastal sea level measurements using a single geodetic GPS receiver. *Adv. Space Res.* **2013**, *51*, 1301–1310. [CrossRef]
16. Chen, Z.; Jin, S. Dynamic response of water level and drought-flood risk assessment at the Datong station of the Yangtze River based on GNSS-IR. *Bull. Surv. Mapp.* **2025**, *11*, 104–109. [CrossRef]
17. Ma, Z.; Zhang, S.; Liu, Q.; Huang, G.W.; Kang, Q.C.; Peng, J.L. Monitoring water level change of the Yellow River by universal GPS receivers. *J. Nanjing Univ. Inf. Sci. Technol. Nat. Sci. Ed.* **2021**, *13*, 187–193. [CrossRef]

18. Song, M.; He, X. High-precision Reservoir Water Level Monitoring Based on GNSS-IR Technology. *Radio Eng.* **2021**, *51*, 1099–1103. [CrossRef]
19. Wang, S.; He, K.; Yan, S.; Hou, J.; Zou, Z. Analysis of GNSS-IR sea surface height retrieval method with different sampling intervals. *J. Navig. Position.* **2025**, *13*, 52–61. [CrossRef]
20. Liu, P.; Chen, T.; Liu, J.; Jia, X. GNSS-IR Sea Level Height Inversion Combining Wavelet Transform with WOA Algorithm. *Radio Eng.* **2023**, *53*, 860–867. [CrossRef]
21. Wang, X.; He, X.; Song, M.; Chen, S.; Niu, Z. Analysis of inter-frequency bias in multi-mode multi-frequency GNSS-IR water level retrieval and correction method. *Acta Geod. Cartogr. Sin.* **2022**, *51*, 2328–2338. [CrossRef]
22. Liu, P.; Zhang, S.; Wang, H.; Jiang, B.; Wu, H.; Xin, R.; Wang, P. GNSS-IR for Monitoring Absolute Sea Level Changes in Near-Coastal Areas. *J. Geod. Geodyn.* 2026, *in press*. [CrossRef]
23. Shan, Q.; Jiang, W.; Chen, Q.; Liu, K.; Zhang, M.; Zou, X. Multi-station Fusion GNSS-IR Water Level Monitoring Based on Robust Estimation Method. *Geomat. Inf. Sci. Wuhan. Univ.* **2026**, *51*, 944–954. [CrossRef]
24. Liu, N.; Jiang, B.; Zhang, S.; Sheng, L.; Zhang, Y.; Wang, H.; Hao, Y.; Liu, P.; Xin, Y. Research on the monitoring of flood water levels and precipitable water vapor using shore-based GNSS. *GNSS World China* **2025**, *50*, 61–69. [CrossRef]
25. Jin, S.G.; Zhang, Q.; Qian, X. New Progress and Application Prospects of Global Navigation Satellite System Reflectometry (GNSS + R). *Acta Geod. Cartogr. Sin.* **2017**, *46*, 1389–1398. [CrossRef]
26. Ye, M.; Jin, S.G.; Jia, Y. Ten-minute sea-level variations from combined multi-GNSS multipath reflectometry based on a weighted iterative least-square method. *IEEE Trans. Geosci. Remote Sens.* **2022**, *60*, 1–10. [CrossRef]
27. Yang, Y.; Song, L.; Xu, T. Robust estimator for correlated observations based on bifactor equivalent weights. *J. Geod.* **2002**, *76*, 353–358. [CrossRef]

Disclaimer/Publisher's Note: The statements, opinions and data contained in all publications are solely those of the individual author(s) and contributor(s) and not of MDPI and/or the editor(s). MDPI and/or the editor(s) disclaim responsibility for any injury to people or property resulting from any ideas, methods, instructions or products referred to in the content.